JACS
JOURNAL OF THE AMERICAN CHEMICAL SOCIETY
pubs.acs.org/JACS
Article

Charge Generation Dynamics in Organic Photovoltaic Blends under One-Sun-Equivalent Illumination Detected by Highly Sensitive Terahertz Spectroscopy

Jiacong Li,[▽] Qing Ji,[▽] Rui Wang,* Zhi-Guo Zhang, Xiaoyong Wang, Min Xiao, Yan-qing Lu,* and Chunfeng Zhang*

Cite This: J. Am. Chem. Soc. 2024, 146, 20312−20322

Read Online

ACCESS | Metrics & More | Article Recommendations | Supporting Information

ABSTRACT: Organic photovoltaic (OPV) devices attain high performance with nonfullerene acceptors by utilizing the synergistic dual channels of charge generation that originate from excitations in both the donor and acceptor materials. However, the specific intermediate states that facilitate both channels are subject to debate. To address this issue, we employ time-resolved terahertz spectroscopy with improved sensitivity ($\Delta E/E < 10^{-6}$), enabling direct probing of charge generation dynamics in a prototypical PM6:Y6 bulk heterojunction system under one-sun-equivalent excitation density. Charge generation arising from donor excitations is characterized with a rise time of ∼9 ps, while that from acceptor excitations shows a rise time of ∼18 ps. Temperature-dependent measurements further reveal notably distinct activation energies for these two charge generation pathways. Additionally, the two channels of charge generation can be substantially manipulated by altering the ratio of bulk to interfaces. These findings strongly suggest the presence of two distinct intermediate states: interfacial and intramoiety excitations. These states are crucial in mediating the transfer of electrons and holes, driving charge generation within OPV devices.

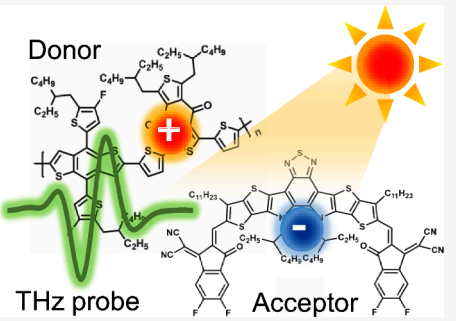

INTRODUCTION

In organic photovoltaic (OPV) devices, the initial stage of photocurrent generation occurs in the active layer of the blend of electron donor (D) and acceptor (A) materials.[1,2] The charge-transfer (CT) electronic states at the D−A interfaces have been regarded as the key intermediates for charge generation in conventional systems of polymer−fullerene D−A blends.[2−4] A large portion of excitons generated in the polymer donor diffuse to the interfaces, form the CT states via electron transfer, and dissociate into free charges. The necessity of interfacial CT states has been under debate in the emergent systems with low-bandgap nonfullerene acceptors (NFAs) of Y-series where efficient charge separation is maintained with small interfacial energy loss.[5−17] Electronic interactions among these molecules configurated in A-DA′D-A structures may dramatically change the energy landscapes of intramoiety and interfacial excited states regulating the charge generation dynamics.[18,19] For excitations in acceptor domains, weakly bound electron−hole pairs with CT characters may be created in the neat films of NFAs, acting as the intermediates for charge separation in the D−A blends through hole transfer without forming CT states.[10,11] Moreover, strong charge polarization effect may further reduce the exciton binding energy,[12] resulting in the free charge generation in the neat NFA film, renewing the possibility of efficient single-component OPV devices.[13] While electron transfer mediated by the CT states at the D−A interfaces have been commonly adopted in describing the charge generation from excitations in donor domains in literatures, the energy of CT states in polymer/NFA blends may be significantly increased by band bending induced by collective effect of acceptors' quadrupole moments near interfaces.[7,14,15] It is argued that D-to-A energy transfer preceding the hole transfer process rather than electron transfer process is responsible for charge separation from excitations in donors.[15,16]

The configurations of the intermediates responsible for charge separation are vital for guiding engineering molecule structures and device architectures toward performance optimization. The debate on this issue is partially caused by the limitation of the optical and electrical methods being adopted to study the dynamics of the key intermediate states in OPV blends.[3,7,15,20−25] The commonly used transient absorption spectroscopy (TAS) with the optical probe holds the merit of ultrafast temporal resolution, but the overlap between the spectral characters of interfacial CT states and free charges makes it difficult to fully clarify the exact nature of the

Received: April 27, 2024
Revised: June 24, 2024
Accepted: June 25, 2024
Published: July 9, 2024

https://doi.org/10.1021/jacs.4c05786
J. Am. Chem. Soc. 2024, 146, 20312−20322

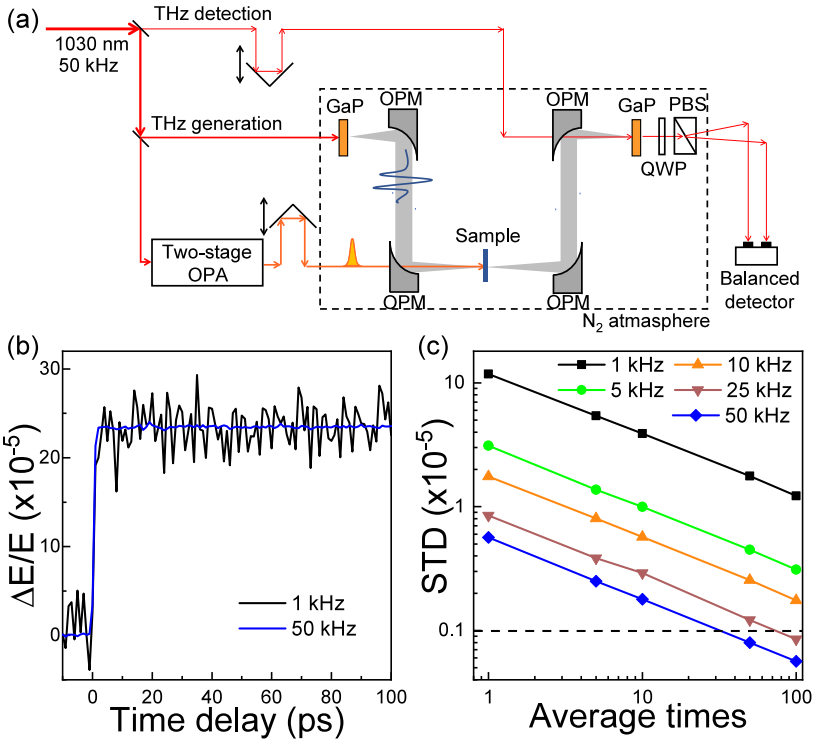

Figure 1. TRTS with improved sensitivity. (a) Schematic diagram of TRTS setup based on a Yb:YGW laser with a high repetition rate. OPM: off-axis parabolic mirror; QWP: quarter-wave plate; PBS: polarization beam splitter. (b) THz dynamics of the standard sample (silicon wafer) detected at 1 kHz and 50 kHz repetition rates. (c) Noises of the setup evaluated by STD ($\Delta E/E$) measured at different repetition rates and averaging times.

intermediate states by TAS.[11,21,22] Electrical methods may selectively probe the free charges induced by photon excitations.[7,26] Nevertheless, the limited temporal resolution is insufficient to distinguish the onset of free charge generation on picosecond time scales. Preserving the advantages of optical and electrical methods, the time-resolved terahertz spectroscopy (TRTS) with sensitivity to free charges with subpicosecond temporal resolution has been established as a powerful tool to characterize the charge carrier dynamics in organic and inorganic semiconductors.[27−37] However, due to low carrier mobilities in OPV materials, terahertz (THz) dynamics of OPV blends are often acquired under relatively large pump fluences (typically >10 μJ/cm^2)[38−44] far beyond the excitation density in a working device under one-sun illumination condition.[7] Therefore, the recorded charge dynamics are assuredly modulated by many-body interactions such as exciton−exciton annihilation[45] and bimolecular charge recombination,[46−48] which are found to be especially important in polymer/NFAs OPV blends.

To tackle the above challenges, we improve the sensitivity of TRTS (ΔE/E) to the level of 10^{-6} using a Yb:KGW laser with a high repetition rate, which enables us to characterize the charge generation dynamics under weak pump with excitation density equivalent to one-sun illumination (~0.2 μJ/cm^2). In the model system of bulk heterojunction (BHJ) of PM6:Y6, we have identified the pathways of charge generation dynamics by selectively exciting the polymer donor and the small molecule acceptor, respectively. The charge generation rates for the two channels are different, and the temperature-dependent measurements reveal distinct thermal activation energies, indicating that two different intermediates are involved in the charge generation processes. Additionally, modifying the ratio between bulk and interfaces in the micromorphologies of as-cast BHJs and planar heterojunctions (PHJs) can substantially affect these channels, as evidenced by a combined study using atom force microscopy (AFM) and TRTS. The experimental data corroborate a dual-channel model for charge separation: electron transfer is mediated by interfacial CT states, and hole transfer occurs through intramoiety delocalized states. These findings underscore the importance of engineering molecule packing to reduce losses in intramoiety and interfacial channels, which is essential for enhancing device performance.

MATERIALS AND METHODS

Time-Resolved Terahertz Spectroscopy. In this study, the laser source employed was a commercial Yb:KGW regenerative amplifier (Pharos, Light Conversion), which produced a pulse train at 1030 nm with a duration of 290 fs and repetition rate up to 50 kHz (Figure 1a). THz radiation was generated by focusing a beam with an energy of 20 μJ/pulse with a spot diameter of ~500 μm through optical rectification in a 1 mm thick GaP (110) nonlinear crystal. Detection of THz radiation was achieved through electro-optic sampling in another GaP (110) nonlinear crystal, utilizing a focused beam with an energy of 450 nJ/pulse. A collimated beam (130 μJ/pulse) was employed to generate the tunable pump beam through a homemade two-stage optical parametric amplifier (OPA). The pump modulation at half of the repetition rate was accomplished by employing an electro-optic modulator (EO-AM-NR-C2, Thorlabs) to modulate the supercontinuum generation within the OPA setup (Figure 1a, Figure S1). The pump and THz probe beams are aligned collinearly onto the sample, with beam diameters of ~4 and ~1.5 mm, respectively. Extraction of the THz signal was carried out using a lock-in amplification technique, employing a time constant of 1 s. Sample temperatures ranging from 250 to 350 K were precisely regulated using thermoelectric cooling chips in combination with heating elements. For nanosecond-resolved TRTS, the pump beam was replaced by a Q-switched Nd:YVO_4 laser (Picolo AOT MOPA,

https://doi.org/10.1021/jacs.4c05786
J. Am. Chem. Soc. 2024, 146, 20312−20322

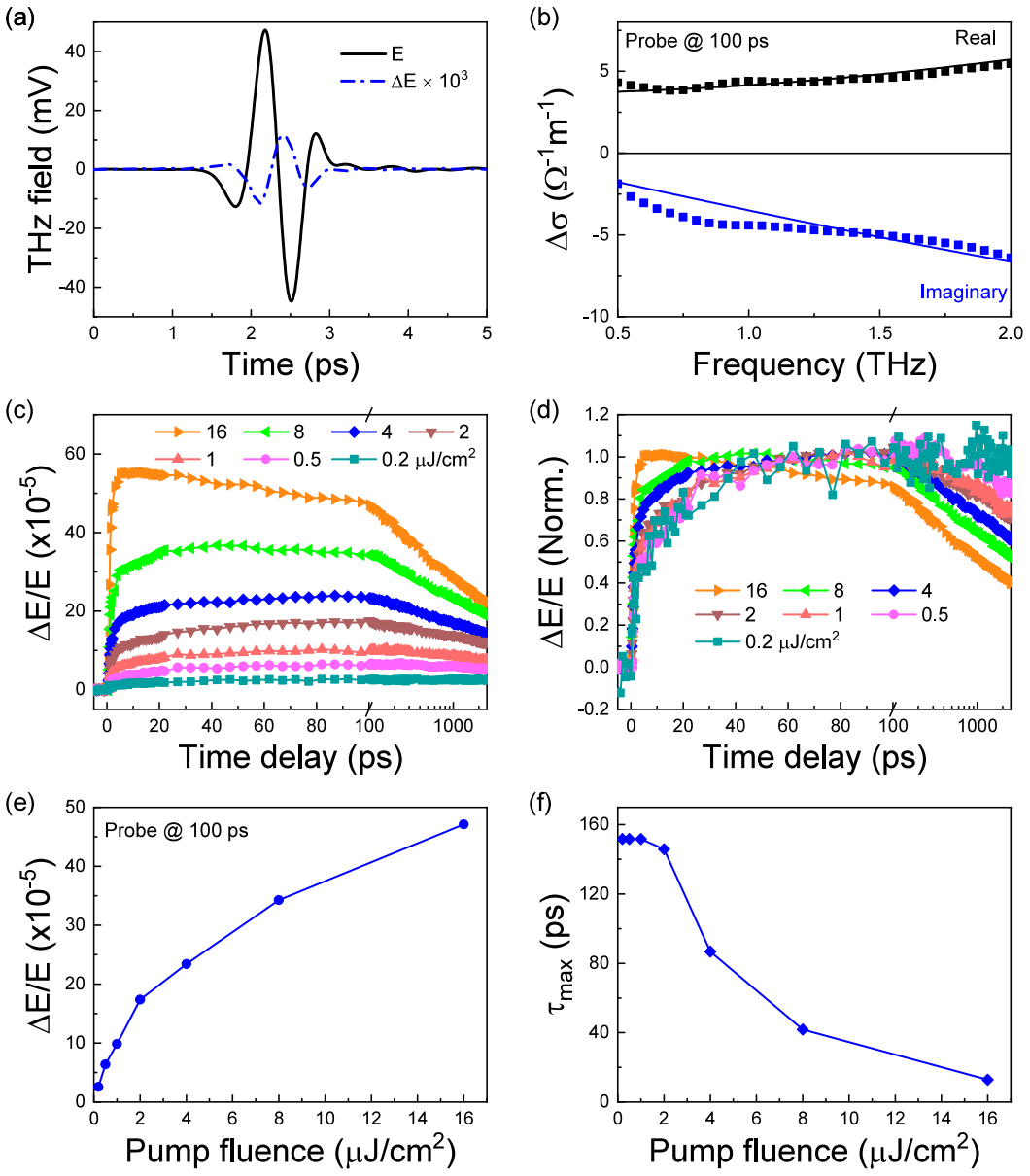

Figure 2. THz response of the blend film of PM6:Y6. (a) THz transmission waveform (E) and the photomodulation of the THz transmission waveform (ΔE) of a PM6:Y6 film probed at pump-delay of 100 ps. (b) Complex photoconductivity spectra of the PM6:Y6 blend film at 100 ps. The solid lines are the fitting curves through the Drude−Smith model. (c) Pump-fluence dependent THz dynamics of the PM6:Y6 blend film. (d) Normalized pump-fluence dependent dynamics of the PM6:Y6 blend film. (e) Amplitude of THz response of PM6:Y6 probed at 100 ps delay at different pump-fluence. (f) Pump-fluence dependent delay time (τ_{max}) when the THz responses reach their maximum.

InnoLas Laser), and synchronized by a digital delay generator (DG645, Stanford Research Systems). All measurements were conducted in a nitrogen-purged environment.

Sample Preparation. In the conducted experiments, two polymer donors, PM6 and PTQ8, were employe with a NFA known as Y6 (Figure S2).[5,8] PM6 is a medium bandgap polymer based on the benzodithiophene-*alt*-benzo[1,2-*b*:4,5-*c*′]dithiophene-4,8-dione backbone. PTQ8 is a derivative of poly(thiophene-quinoxaline) with two fluorine substituents attached to its thiophene D-unit. The small-molecule NFA, Y6, incorporates an electron-deficient, centrally fused conjugated ring (dithienthiophen[3.2-*b*]-pyrrolobenzothiadiazole) flanked with 2-(5,6-difluoro-3-oxo-2,3-dihydro-1*H*-inden-1-ylidene)-malononitrile end-capping units. PM6 and Y6 were procured from Solarmer Materials Inc., while PTQ8 was synthesized following a previously reported protocol.[8] BHJ blend samples of PM6:Y6 and PTQ8:Y6 were prepared with a donor to acceptor mass ratio of 1:1.2, at a total concentration of 20 mg/mL in chloroform (CF). The BHJ layer was processed by spin-coating onto a 1 mm-thick fused silica substrate from its solution. PHJ blend samples of PM6/Y6 were prepared using a two-step process with orthogonal solvents.[49] PM6 and Y6 were dissolved in CF and tetrahydrofuran (THF) solvents, respectively, at a concentration of 10 mg/mL each. First, the PM6 layer was spin-coated onto a substrate from its solution. Subsequently, the Y6 layer was spin-coated onto the PM6 layer from its solution. Additionally, a neat film of Y6 was spin-coated from its CF solution. Except for the as-cast BHJ, all film samples underwent annealing under an argon atmosphere at 110 °C for a duration of 10 min. The morphologies of the film samples were checked by AFM (NX10, Park systems).

RESULTS

A high sensitivity of TRTS system is crucial for capturing the weak THz response of free charges in OPV samples. TRTS characterizes the change in the transmitted THz electric field

https://doi.org/10.1021/jacs.4c05786
J. Am. Chem. Soc. 2024, 146, 20312−20322

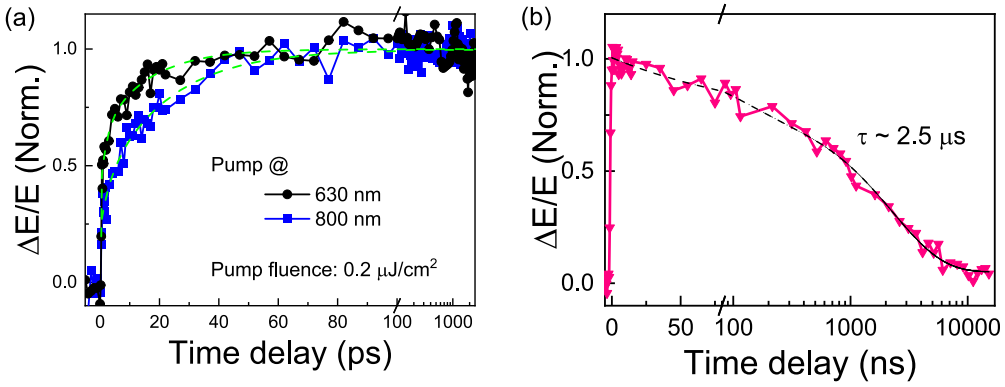

Figure 3. Charge generation and recombination dynamics under one-sun-equivalent excitation. (a) Normalized THz dynamics for the PM6:Y6 blend excited at 630 and 800 nm, respectively, with pump fluence of ~0.2 μJ/cm^2 with subpicosecond resolution. (b) Ns-resolved THz dynamics on the long-time scale show the recombination dynamics with similar excitation density. The data were recorded by synchronizing a ns laser at 532 nm with the THz probe (Figure S6).

(ΔE) induced by the pump with respect to the THz field (E).[27,44] The value of $\Delta E/E$ is directly proportional to the variation of photoconductivity ($\Delta\sigma$), which, in turn, is related to the photoinduced charge density (Δn) and charge mobility (μ) ($-\Delta E/E \propto \Delta\sigma \propto \Delta n\mu$).[27,50] Consequently, the accuracy of measuring ΔE primarily establishes the lower limit for evaluating $\Delta\sigma$.

In principle, this error can be reduced by a factor of $N^{1/2}$ by averaging N measurements. Nevertheless, simply increasing the sampling size (N) with the commonly used 1 kHz system is impractical due to time constraints, especially when characterizing the response under one-sun illumination. For the step-scan averaging approach to capture the THz spectrum at a specific time delay,[51] the high repetition system can also significantly improve the efficiency of noise reduction.

To enhance sensitivity, we have adopted a laser system of Yb:KGW amplifier with a high repetition rate up to 50 kHz for THz generation and detection using GaP crystals (Figure 1a).[52] THz generation with GaP crystals at 1030 nm is advantageous due to reduced group velocity mismatch between 1030 nm and THz wavelengths in the GaP crystal. In compared to 800 nm, the damage threshold of GaP crystal is higher at 1030 nm, benefiting from lower excess energy for two-photon absorption. The amplitude of THz field using GaP crystals at 1030 nm is comparable to that generated with a Ti:sapphire laser at 800 nm using ZnTe crystals. A higher repetition rate significantly reduces the measurement time and allows for the use of high modulation frequencies in lock-in detection to suppress noise effectively. Furthermore, the increased value of E captured by lock-in detection with the higher repetition rate can substantially reduce the error in evaluating $\Delta E/E$ since the electric component contributes significantly to the measurement error. These advantages lead to a substantial improvement in detection sensitivity, as confirmed by measuring the transient photoconductivity on a silicon wafer (Figure 1b).

We quantify the noise level in the setup by measuring the standard deviation (STD) of $\Delta E/E$ without the optical pump (Figure 1c). The experiments were conducted with modulation frequencies at half of the laser repetition rates, using the electro-optical modulator integrated in the home-built optical parametric amplifier (details in the Supporting Information (SI), Figure S1). As depicted in Figure 1c, the noise level is reduced by a factor of $N^{1/2}$ with increasing the sampling size N. Increasing the repetition rate is more efficient in reducing noise, with the STD decreasing by a factor of ~20 when the repetition rate is increased from 1 to 50 kHz. This enables the sensitivity of TRTS to reach levels better than 10^{-6}, enabling the capture of weak signals.

Figure 2 shows the THz response in a blend film of PM6:Y6 upon pump at 800 nm. In principle, the THz response may be contributed by motion of mobile charges and exciton polarizability.[40,53] The photoinduced spectral change can be well produced by the Drude−Smith model for mobile charges (Figure 2a,b, SI).[27] The temporal traces probed at the peak and zero-crossing point of THz waveform are nearly the same (Figure S3). In addition, the waveforms of the photoinduced THz response are independent of the delay time within the time window of ~1 ns (Figure S3). These results suggest that the THz response is mainly caused by the motion of mobile charges induced by the absorbed light.[44] The temporal traces of THz response represent the dynamics of free charges generated in the blend film.

The dynamics of THz response is strongly dependent on the excitation density (Figure 2c). With increasing the pump fluence, the recombination becomes more faster owing to many-body effects including the bimolecular process. For high pump fluence >10 μJ/cm^2, the THz dynamics shows a decay following the onset of THz response on the time scale comparable to the instrumental response (Figure 2c,d), which is consistent with the literature results on polymer/fullerene blends.[40,54] Benefiting from the improved sensitivity of TRTS, we can probe the dynamics of THz response of the OPV blend film under weak pump. Apparently, a delay rise becomes more predominant in the dynamics trace when excitation density decreases (Figure 2c,d). The observed delay rise under weak excitation represents the intrinsic dynamics of charge generation upon optical excitation. Figure 2e,f plots the excitation fluence-dependent signal amplitudes at 100 ps and time delays when the signals reach a maximum value (τ_{max}). The THz amplitudes are nearly linear dependent on the pump fluence in the range <2 μJ/cm^2 where the values of τ_{max} keep nearly unchanged, implying that it is necessary to keep the excitation fluence on the scale of ~2 μJ/cm^2 or weaker for a quantitative analysis of the charge generation dynamics. Similar fluence-dependent THz dynamics are also observed under donor excitation at 630 nm (Figure S4), while charge

https://doi.org/10.1021/jacs.4c05786
J. Am. Chem. Soc. 2024, 146, 20312−20322

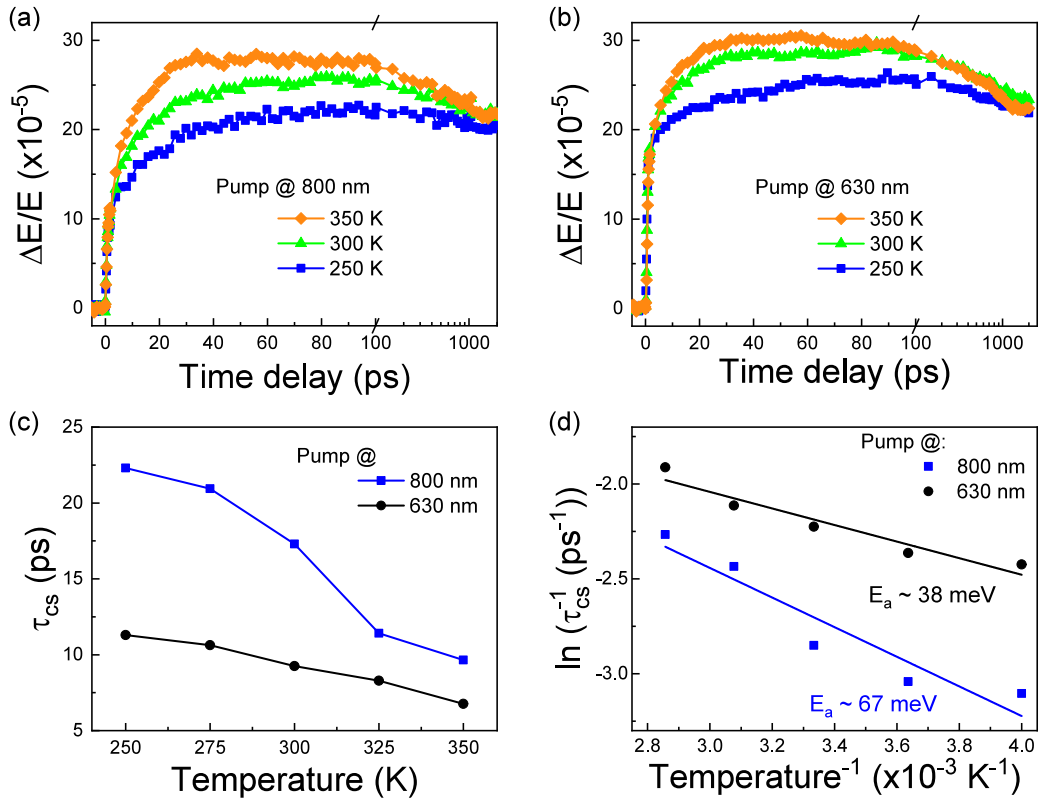

Figure 4. Temperature dependence of charge generation dynamics. TRTS dynamics of the charge generation processes of PM6:Y6 via (a) hole and (b) electron transfer channels at 800 and 630 nm pump respectively of different temperatures. (c) Rise time of charge generation processes (τ_{cs}) via hole and electron transfer channels decrease with the lower temperatures. (d) Temperature-dependent charge separation of hole and electron transfer channels can be well fitted by the Arrhenius model. The extracted charge separation activation energy of the electron transfer channel is much smaller than that of the hole transfer channel.

generation on a sub-100 ps temporal scale remains largely unaffected with excitation below 2 μJ/cm^2 (Figure S5).

For one-sun illumination, the excitation density is ~3 × 10^{22} m^{-3} in a typical device with an active layer of PM6:Y6 blend,[7] corresponding to the excitation fluence of ~0.2 μJ/cm^2 for pulse pump (see SI for details). To characterize the charge generation dynamics at operational excitation density, we acquire the temporal traces of THz response with selective excitation of the polymer donor PM6 and the small molecule acceptor Y6 at 630 and 800 nm, respectively (Figure 3a). To achieve a similar signal-to-noise ratio using the conventional 1 kHz THz system, it is necessary to significantly increase the excitation density or extend the averaging time. For both donor and acceptor excitations, the rising edges of THz signals consist of two main components: a small, sudden rise occurring within the temporal scale of instrumental response, and a significant delay-rise component taking place within 100 ps. The delay rise components can be safely assigned to charge separation from the photoinduced excitons in polymer donors or small molecule acceptors. The recombination dynamics of charge carriers in a later temporal window are characterized by nanosecond-resolved TRTS (Figure 3b and Figure S6). The excitation density dependency of THz dynamics is consistent with the bimolecular recombination of free charges.[48] The decay lifetime of free charges was estimated to be around 2.5 μs upon weak excitation density equivalent to one sun illumination (see SI for details).

Notably, the kinetic of charge separation is much faster from excitations in polymer donors than excitations in small molecule acceptors. By exponential fitting, the extracted rise time of charge generation (τ_{cs}) are ~9 and ~18 ps for the two different processes, respectively. In principle, the accelerated charge generation dynamics may be affected by the excess energy at 630 nm excitation.[55,56] However, this effect can be ruled out by the same THz dynamics measured at different pump wavelengths when only the acceptor Y6 can be excited (Figure S7). Furthermore, it is unlikely that the primary cause of the observed differences in kinetics between the two pathways is the exciton transport in different phases of PM6 and Y6. This is due to the extensive exciton diffusion lengths in NFAs as reported in literatures.[57−59] This assessment is further supported by the similar THz dynamics observed in blends with varying D:A ratios (Figure S8). The significant disparity in the signal rise time implies that different intermediate states may be involved in charge generation from excitations in donors and acceptors, which is consistent with the different spectra of the intermediate states as characterized by TAS (Figure S9).

We perform temperature-dependent TRTS measurements toward more in-depth understanding of charge separation channels from excitations in donors and acceptors. The recorded THz dynamics upon selectively exciting the acceptor or donor at different temperatures are shown in Figure 4a,b, respectively. For both channels, THz signals increase significantly faster in conjunction with larger signal amplitudes at higher temperatures (Figure 4a,b), implying that thermal activation plays a pivotal role in facilitating charge separation.[21] The temperature dependence shows markedly difference

https://doi.org/10.1021/jacs.4c05786
J. Am. Chem. Soc. 2024, 146, 20312−20322

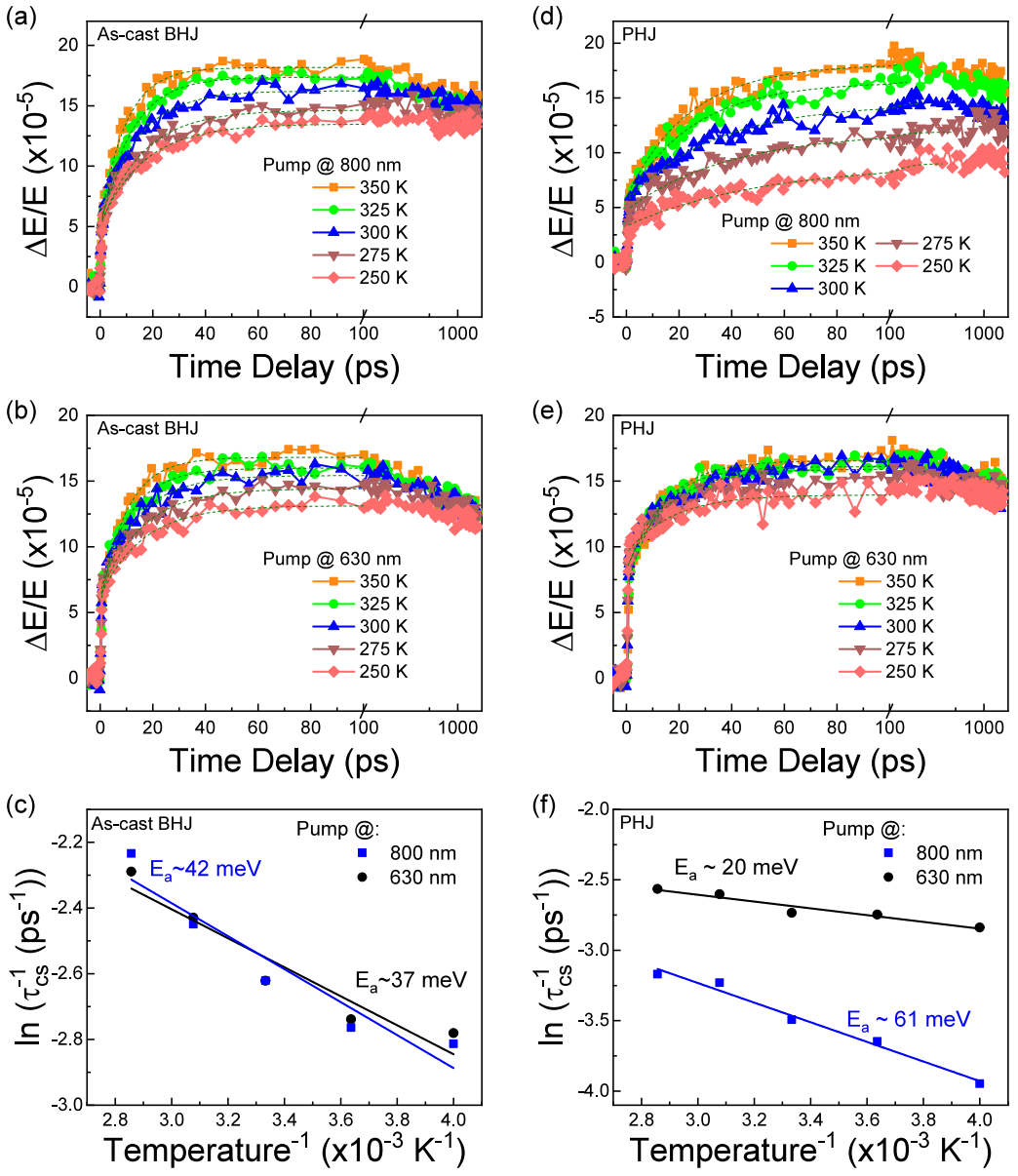

Figure 5. TRTS dynamics of the charge generation processes of the as-cast BHJ and PHJ PM6:Y6 films via (a, d) hole and (b, e) electron transfer channels at 800 and 630 nm pump, respectively, of different temperatures. (c, f) Arrhenius model is used to extract the charge separation activation energies of hole and electron transfer channels.

between charge generation dynamics initiated from excitations in the donor and acceptor. The rate parameter for charge generation from the acceptor excitation is more susceptible to the temperature (Figure 4c). To quantify the difference, we evaluate the activation by the Arrhenius eq (Figure 4d) as

$$k_{cs} = \frac{1}{\tau_{cs}} = k_0 \exp\left(\frac{-E_a}{k_B T}\right) \quad (1)$$

where T is the temperature, k_B is the Boltzmann constant, E_a is the activation energy, and k_0 is the pre-exponential factor. The thermal activation energies extracted for the two charge separation channels originating from excitations within the donor and acceptor are approximately 38 and 67 meV, respectively. The variance in thermal activation energies between the two channels likely stems from the involvement of distinct intermediates. Instead of following a sequential process initiated by energy transfer from donor to acceptor, the generation of charges from donor excitations is facilitated by the electron transfer process mediated by interfacial CT states. Conversely, in the case of acceptor excitations, charge separation is made possible by the hole transfer process, which is mediated by the delocalized excitations within the acceptor moiety.[10,18] These distinct intermediates possess varying free energy levels, accounting for the differences in activation energies observed in the temperature-dependent measurements.

For comparison, we performed control experiments on a fullerene-based OPV blend of PM6:$PC_{71}BM$. In the polymer/fullerene systems, charge separation primarily occurs through an the interfacial CT mediated pathway.[2] Experimental data indicate that the THz dynamics are consistent, regardless of whether excitation occurs at the donor or acceptor (Figure S10). Additionally, temperature-dependent experiments show similar activation energies for both donor and acceptor

https://doi.org/10.1021/jacs.4c05786
J. Am. Chem. Soc. 2024, 146, 20312−20322

excitation (Figure S11). These findings consistently support a coincident charge separation mechanism in fullerene systems. The rise time of charge generation in OPV blends with Y-series NFAs is slower than that in polymer/fullerene acceptors, suggesting that intermolecular interactions in NFA domains play an important role.

The morphology of the blend is widely recognized as a crucial parameter influencing the dynamics of excited states in OPV films.[57,60−62] To ensure morphologies similar to those found in practical devices, we conducted AFM measurements on PM6:Y6 films with different thicknesses (Figure S12, SI). The AFM results showed consistent micromorphologies in the three films of varying thicknesses (110, 150, and 200 nm) with similar surface roughness (∼0.6 nm) and domain sizes (∼20 nm). Additionally, the THz dynamics following donor or acceptor excitation were found to be independent of film thickness (Figure S13), corroborating with the consistent morphologies observed in AFM experiments. These findings demonstrate that THz dynamics are unaffected by film thickness, accurately reflecting the underlying mechanisms in an optimized device and aligning with the thickness tolerance observed in OPV devices with NFAs.[57,60,63]

The above results distinctly highlight the vital roles that both interfacial and intramoiety excitonic configurations play in charge generation within PM6:Y6 blends optimized for devices. In D:A blend systems, the progression of excitations is controlled by either intramoiety or interfacial excitonic coupling. Manipulating the morphology to achieve a balance between the interfacial and bulk regions is crucial for synergizing potential pathways for electron and hole transfer processes. To evaluate the impact of interfacial morphology, we conducted controlled experiments on as-cast BHJ and layer-by-layer processed PHJ films, comparing them with the above-discussed optimized annealed PM6:Y6 BHJ films. The as-cast BHJ film exhibited a higher interface-to-bulk ratio and significantly smaller domain sizes (∼12 nm), as confirmed by AFM measurements (Figure S14). Additionally, orthogonal solvents were used in the fabrication of the PHJ film, resulting in a significant reduction of D:A interfaces.[49]

The effects of morphology on the charge generation dynamics in the samples are manifested as different temperature-dependent THz dynamics upon donor and acceptor excitations, as illustrated in Figure 5. Notably, both pump conditions displayed similar temperature dependencies in the as-cast BHJ film (Figure 5a,b), indicating a significant reduction in the dynamic disparity between electron and hole transfer pathways. In contrast, in the PHJ film, the temperature dependence of electron transfer weakened, while that of hole transfer strengthened (Figure 5d,e). These findings are supported by comparable activation energies (37 meV for electron transfer and 42 meV for hole transfer) observed in the as-cast BHJ film, compared to distinct activation energies (20 meV for electron transfer and 61 meV for hole transfer) observed in the PHJ film (Figure 5c,f). In the as-cast BHJ, excitations are more likely generated around the interfaces, where strong interfacial coupling could lead to rapid energy transfer from donor to acceptor,[15,16] and minimize kinetic differences between donor or acceptor excitations. However, in PHJ films with reduced D:A interfaces, excitations primarily arise from intramoiety electronic coupling. The variation in intermolecular coupling within donor or acceptor domains results in excitations with diverse configurations, thereby leading to divergent charge generation kinetics following either donor or acceptor excitation. Comparing the temperature-dependent THz dynamics of the optimized annealed BHJ shown in Figure 4, we observe that the activation energy for hole transfer is similar to that in PHJ films, highlighting the significant role of intramoiety states within the acceptor domain. Nevertheless, the activation energy for electron transfer closely aligns with that of as-cast BHJs, emphasizing the critical influence of interfacial states. Additionally, we find that as-cast BHJs exhibit the lowest activation energy for hole transfer, implying that enhanced disorder-induced entropy can facilitate the separation of intramoiety excitations.[64,65] In contrast, PHJs display the lowest activation energy for electron transfer, suggesting that different band bending effects caused by varied interfacial micromorphologies may influence the energy of CT excitations.[66,67] These findings underscore the importance of achieving a delicate equilibrium between interfacial and intramoiety excitonic coupling through morphological control to enhance efficient charge generation dynamics.

By comparing the three PM6:Y6 films with distinct morphologies, we observe that the dominant factor determining the hole transfer channel is the intramoiety coupling. Specifically, in acceptor Y6, photon excitation leads to local excitations (LEs), which can undergo two charge separation pathways mediated by either the intramoiety state (iEX) or the CT state (Figure S15). Due to different excitation configurations of these intermediate states, it is evident that iEX-mediated and CT-mediated charge separation pathways occur along distinct reaction coordinates. The smaller nuclear displacement between LE and iEX suggests a potentially faster conversion from LE to iEX compared to LE to CT in Y6 aggregations. Consequently, CT-mediated charge separation plays a subordinate role in this process. The activation energies for dissociation of iEX and CT into free charges are determined by energy differences relative to potential energy surface crossover points for each respective state. We hypothesize that there may be a larger nuclear displacement between iEX and CS compared to that between CT and CS, resulting in a higher E_a for the iEX-mediated charge separation pathway (Figure S15). Furthermore, at D:A interfaces where acceptor molecules possess large quadrupole moments, energy bending could lead to elevated CT energies,[7,15,68] which enhance wave function delocalization of CT states and further reduce charge separation barriers. In addition to similar entropy increase effects observed in fullerene-based OPV systems, electronic polarization effects in NFAs also decrease free energy of the CS state potentially explaining extremely low activation energies observed here.[12]

DISCUSSION

Previous works have argued that free charge generation can be accomplished in the neat component of acceptor Y6.[13] In the pure Y6 film, the THz response simultaneously reaches its maximum following photon excitation, which is markedly distinct from the gradual increase in THz response observed in the PM6:Y6 blend (Figure S16a). The presence of a nonzero THz signal in the pure Y6 film suggests that charge separation occurs in the individual component,[13] which is possibly caused by the symmetry breaking between two adjacent Y6 molecules. However, the recorded THz response from the pure Y6 film is merely around 10% of that observed in the blend. Similarly, a comparably low THz response is also noted when exciting the donor component in the pure PM6 film (Figure S17). These

https://doi.org/10.1021/jacs.4c05786
J. Am. Chem. Soc. 2024, 146, 20312−20322

consistent findings strongly suggest that D:A interfaces play a pivotal role in the generation of the majority of mobile charges in the active layer of blend PM6:Y6. When blending with the polymer donor PTQ8 in a straddled band alignment (Figure S16b),[8] the THz dynamics is similar to that in the neat Y6 film, indicating that energy alignment at the D:A interface is of significance in generating mobile charges. The increased energy of the charge-separated (CS) state in the PTQ8:Y6 blend surpasses that of excitations in the acceptor, which blocks the thermal conversion from intramoiety excitation to the CS state and results in diminished charge generation efficiency. The weak THz response in the neat film is possibly limited by the small portion of excitations converted into free charges or the limited charge mobility.[27] For both cases, the interaction between positive and negative polarons cannot be fully ignored. The molecular packing in the film is inhomogeneous, which may cause diverse energy landscape, resulting in different degree of electron−hole binding of multiple configured excitations.[19] These charges in the neat films recombine much faster than the separated charges in the blend films. Toward photocurrent generation, doping with proper polymer donor allows efficient charge separation through the hole transfer channel. In principle, the THz response observed in both neat PM6 and Y6 films may also be attributed to changes in polarizability. However, this possibility can be ruled out due to the presence of a nonzero real part combined with a Drude−Smith-like spectra profile of THz signals in both neat films (Figure S18).

It is worth noting that the nonequilibrium effect of charge mobility is possibly essential on the time scale of charge separation in the blend film.[33,69] Under one-sun illumination, the charge mobility estimated by THz measurement is evaluated to be on the order of 0.1−1 $cm^2\ V^{-1}\ s^{-1}$ if all the excitations are assumed to be converted into free charges. This value is orders of magnitude higher than the value characterized by static measurements as commonly observed in polymer/fullerene systems.[70,71] The mobility on the short time scale is also dependent on temperature which is plausibly responsible for the increased magnitude of THz response when temperature increases (Figure 4a,b).

We observe similar excitation density-sensitive dynamic behaviors in other high-performance systems using Y6 derivatives, confirming the necessity of using weak excitation to quantify the charge generation rate in OPV systems with NFAs. The TRTS results at low excitation densities acquired in this work have immediate implications on fully understanding the intrinsic charge generation mechanisms of NFA-based OPV blends. In both hole transfer and electron transfer channels, we find that the activation energies are on the order of several tens of meV, which are much lower than the binding energy of neighboring electrons and holes at D:A interfaces.[2,64] Owing to the wave function delocalization of electrons and holes,[18,72] the charge separation mediated by weakly bound excitations may avoid the formation of tightly bound CT states at the interface,[11] which may account for the efficient charge generation at low driving forces of OPV blends with NFAs. Moreover, we note that a portion of THz signals are generated within the system time resolution in both hole transfer and electron transfer channels (Figure 3a), suggesting ultrafast charge generation can take place in the PM6:Y6 blend film.[54] While overall performance of an OPV device is also sensitive to multiple factors over a longer time scale, the fast charge generation can effectively compete exciton energy loss at the early stage. The fast-rising edge of THz dynamics in the blend is not merely from the signal of the direct excitation of the donor or the acceptor, which is supported by the much-lowered signals recorded in neat Y6 and PM6 films (Figures S16 and S17). The charge generation within 1 ps may arise from the ultrafast long-range charge separation induced by the excitation delocalization.[18,73] Nevertheless, TRTS with improved time resolution may be developed to further investigate the mechanism of the femtosecond charge generation process in the future.

CONCLUSIONS

In summary, we have developed a highly sensitive TRTS system with a remarkable $\Delta E/E$ sensitivity better than 10^{-6}. This system enables us to elucidate the intrinsic dynamics of free charge generation in OPV blends under near-solar illumination conditions. In the model PM6:Y6 blend film, we observe that processes of charge generation through electron and hole transfer channels are facilitated by distinct intermediate states. This results in different THz dynamics and activation energies associated for each channel. Moreover, it has been demonstrated that both interfacial and bulk morphologies play a crucial role in governing the evolution of excitations, including energy transfer and charge transfer. These findings strongly suggest that the intermediate states, both interfacial and intramoiety excitations, are pivotal for the operation and future optimization of devices.

ASSOCIATED CONTENT

Supporting Information

The Supporting Information is available free of charge at https://pubs.acs.org/doi/10.1021/jacs.4c05786.

Additional experimental details; model fitting of complex photoinduced conductivity spectra; additional THz data of the PM6:Y6 blend; evaluation of one-sun-illumination equivalent excitation density; TA data of PM6:Y6 with the pump fluence at 0.2 $\mu J/cm^2$; Control experiments on the blend of PM6:$PC_{71}BM$; morphology study of PM6:Y6 films with different thicknesses; AFM results of an as-cast BHJ of PM6:Y6; scheme diagram of the charge separation mechanism in PM6:Y6; THz dynamics of PTQ8:Y6 blend and neat Y6 films; THz dynamics of PM6:Y6 blend and neat PM6 films at 630 nm excitation; THz spectra of neat PM6 and Y6 films (PDF)

AUTHOR INFORMATION

Corresponding Authors

Rui Wang − *National Laboratory of Solid State Microstructures, School of Physics, and Collaborative Innovation Center for Advanced Microstructures, Nanjing University, Nanjing 210093, China; College of Physics, Nanjing University of Aeronautics and Astronautics, and Key Laboratory of Aerospace Information Materials and Physics (NUAA), MIIT, Nanjing 211106, China; Institute of Materials Engineering, Nanjing University, Nantong, Jiangsu 226019, China;* orcid.org/0000-0002-0670-4207; Email: rui_wang@nuaa.edu.cn

Yan-qing Lu − *National Laboratory of Solid State Microstructures, Key Laboratory of Intelligent Optical Sensing and Manipulation, College of Engineering and Applied Sciences, and Collaborative Innovation Center of Advanced*

Microstructures, Nanjing University, Nanjing 210023, China; orcid.org/0000-0001-6151-8557; Email: yqlu@nju.edu.cn

Chunfeng Zhang − *National Laboratory of Solid State Microstructures, School of Physics, and Collaborative Innovation Center for Advanced Microstructures, Nanjing University, Nanjing 210093, China; Institute of Materials Engineering, Nanjing University, Nantong, Jiangsu 226019, China;* orcid.org/0000-0001-9030-5606; Email: cfzhang@nju.edu.cn

Authors

Jiacong Li − *National Laboratory of Solid State Microstructures, School of Physics, and Collaborative Innovation Center for Advanced Microstructures, Nanjing University, Nanjing 210093, China;* orcid.org/0009-0002-3926-521X

Qing Ji − *National Laboratory of Solid State Microstructures, School of Physics, and Collaborative Innovation Center for Advanced Microstructures, Nanjing University, Nanjing 210093, China*

Zhi-Guo Zhang − *State Key Laboratory of Organic/Inorganic Composites, Beijing Advanced Innovation Center for Soft Matter Science and Engineering, Beijing University of Chemical Technology, Beijing 100029, China;* orcid.org/0000-0003-4341-7773

Xiaoyong Wang − *National Laboratory of Solid State Microstructures, School of Physics, and Collaborative Innovation Center for Advanced Microstructures, Nanjing University, Nanjing 210093, China;* orcid.org/0000-0003-1147-0051

Min Xiao − *National Laboratory of Solid State Microstructures, School of Physics, and Collaborative Innovation Center for Advanced Microstructures, Nanjing University, Nanjing 210093, China; Department of Physics, University of Arkansas, Fayetteville, Arkansas 72701, United States*

Complete contact information is available at: https://pubs.acs.org/10.1021/jacs.4c05786

Author Contributions

[▽]J.L. and Q.J. contributed equally to this work.

Notes

The authors declare no competing financial interest.

■ ACKNOWLEDGMENTS

This work is supported by the National Key R&D Program of China (Grant Nos. 2022YFB3206900 and 2022YFA1403602), the National Science Foundation of China (Grant NOs. 22225305, 21922302, 21873047, and 22273039), People's Livelihood Project of Nantong City grant no. MS22022066, the Science and Technology Project of Nantong City (JC2023003), and the Fundamental Research Funds for the Central University (NE2024010). The authors acknowledge Dr. Xuewei Wu for providing technical assistance.

■ REFERENCES

(1) Yu, G.; Gao, J.; Hummelen, J. C.; Wudl, F.; Heeger, A. J. Polymer photovoltaic cells: Enhanced efficiencies via a network of internal donor-acceptor heterojunctions. *Science* **1995**, *270*, 1789.

(2) Clarke, T. M.; Durrant, J. R. Charge photogeneration in organic solar cells. *Chem. Rev.* **2010**, *110*, 6736.

(3) Stoltzfus, D. M.; Donaghey, J. E.; Armin, A.; Shaw, P. E.; Burn, P. L.; Meredith, P. Charge generation pathways in organic solar cells: Assessing the contribution from the electron acceptor. *Chem. Rev.* **2016**, *116*, 12920.

(4) Qian, D.; Zheng, Z.; Yao, H.; Tress, W.; Hopper, T. R.; Chen, S.; Li, S.; Liu, J.; Chen, S.; Zhang, J.; et al. Design rules for minimizing voltage losses in high-efficiency organic solar cells. *Nat. Mater.* **2018**, *17*, 703.

(5) Yuan, J.; Zhang, Y.; Zhou, L.; Zhang, G.; Yip, H.-L.; Lau, T.-K.; Lu, X.; Zhu, C.; Peng, H.; Johnson, P. A.; et al. Single-junction organic solar cell with over 15% efficiency using fused-ring acceptor with electron-deficient core. *Joule* **2019**, *3*, 1140.

(6) Sun, C.; Qin, S.; Wang, R.; Chen, S.; Pan, F.; Qiu, B.; Shang, Z.; Meng, L.; Zhang, C.; Xiao, M.; et al. High efficiency polymer solar cells with efficient hole transfer at zero highest occupied molecular orbital offset between methylated polymer donor and brominated acceptor. *J. Am. Chem. Soc.* **2020**, *142*, 1465.

(7) Perdigón-Toro, L.; Zhang, H.; Markina, A.; Yuan, J.; Hosseini, S. M.; Wolff, C. M.; Zuo, G.; Stolterfoht, M.; Zou, Y.; Gao, F.; Andrienko, D.; Shoaee, S.; Neher, D.; et al. Barrierless free charge generation in the high-performance pm6:Y6 bulk heterojunction non-fullerene solar cell. *Adv. Mater.* **2020**, *32*, No. 1906763.

(8) Sun, C.; Pan, F.; Chen, S.; Wang, R.; Sun, R.; Shang, Z.; Qiu, B.; Min, J.; Lv, M.; Meng, L.; Zhang, C.; Xiao, M.; Yang, C.; Li, Y.; et al. Achieving fast charge separation and low nonradiative recombination loss by rational fluorination for high-efficiency polymer solar cells. *Adv. Mater.* **2019**, *31*, No. 1905480.

(9) Nguyen, T. Q. Barrier to charge generation. *Nat. Energy* **2022**, *7*, 1120.

(10) Wang, R.; Zhang, C.; Li, Q.; Zhang, Z.; Wang, X.; Xiao, M. Charge separation from an intra-moiety intermediate state in the high-performance pm6:Y6 organic photovoltaic blend. *J. Am. Chem. Soc.* **2020**, *142*, 12751.

(11) Li, Q.; Wang, R.; Zhang, C. The dynamics of delocalized excitations in organic solar cells with nonfullerene acceptors. *J. Phys. Chem. Lett.* **2023**, *14*, 3031.

(12) Tu, Z.; Han, G.; Yi, Y. Barrier-free charge separation enabled by electronic polarization in high-efficiency non-fullerene organic solar cells. *J. Phys. Chem. Lett.* **2020**, *11*, 2585.

(13) Price, M. B.; Hume, P. A.; Ilina, A.; Wagner, I.; Tamming, R. R.; Thorn, K. E.; Jiao, W.; Goldingay, A.; Conaghan, P. J.; Lakhwani, G.; Davis, N. J. L. K.; Wang, Y.; Xue, P.; Lu, H.; Chen, K.; Zhan, X.; Hodgkiss, J. M.; et al. Free charge photogeneration in a single component high photovoltaic efficiency organic semiconductor. *Nat. Commun.* **2022**, *13*, 2827.

(14) Khan, J. I.; Alamoudi, M. A.; Chaturvedi, N.; Ashraf, R. S.; Nabi, M. N.; Markina, A.; Liu, W.; Dela Peña, T. A.; Zhang, W.; Alévêque, O.; Harrison, G. T.; Alsufyani, W.; Levillain, E.; De Wolf, S.; Andrienko, D.; McCulloch, I.; Laquai, F.; et al. Impact of acceptor quadrupole moment on charge generation and recombination in blends of idt-based non-fullerene acceptors with pce10 as donor polymer. *Adv. Energy Mater.* **2021**, *11*, No. 2100839.

(15) Karuthedath, S.; Gorenflot, J.; Firdaus, Y.; Chaturvedi, N.; De Castro, C. S. P.; Harrison, G. T.; Khan, J. I.; Markina, A.; Balawi, A. H.; Pena, T. A. D.; et al. Intrinsic efficiency limits in low-bandgap non-fullerene acceptor organic solar cells. *Nat. Mater.* **2021**, *20*, 378.

(16) Chen, Z.; He, C.; Ran, P.; Chen, X.; Zhang, Y.; Zhang, C.; Lai, R.; Yang, Y.; Chen, H.; Zhu, H. Ultrafast energy transfer from polymer donors facilitating spectral uniform photocurrent generation and low energy loss in high-efficiency nonfullerene organic solar cells. *Energy Environ. Sci.* **2023**, *16*, 3373.

(17) Chen, Z.; Zhu, H. Photoinduced charge transfer and recombination dynamics in star nonfullerene organic solar cells. *J. Phys. Chem. Lett.* **2022**, *13*, 1123.

(18) Zhang, G.; Chen, X. K.; Xiao, J.; Chow, P. C. Y.; Ren, M.; Kupgan, G.; Jiao, X.; Chan, C. C. S.; Du, X.; Xia, R.; Chen, Z.; Yuan, J.; Zhang, Y.; Zhang, S.; Liu, Y.; Zou, Y.; Yan, H.; Wong, K. S.; Coropceanu, V.; Li, N.; Brabec, C. J.; Bredas, J. L.; Yip, H. L.; Cao, Y.; et al. Delocalization of exciton and electron wavefunction in non-

fullerene acceptor molecules enables efficient organic solar cells. *Nat. Commun.* **2020**, *11*, 3943.
(19) Hestand, N. J.; Spano, F. C. Expanded theory of h- and j-molecular aggregates: The effects of vibronic coupling and intermolecular charge transfer. *Chem. Rev.* **2018**, *118*, 7069.
(20) Dimitriev, O. P. Dynamics of excitons in conjugated molecules and organic semiconductor systems. *Chem. Rev.* **2022**, *122*, 8487.
(21) Hinrichsen, T. F.; Chan, C. C. S.; Ma, C.; Paleček, D.; Gillett, A.; Chen, S.; Zou, X.; Zhang, G.; Yip, H. L.; Wong, K. S.; Friend, R. H.; Yan, H.; Rao, A.; Chow, P. C. Y.; et al. Long-lived and disorder-free charge transfer states enable endothermic charge separation in efficient non-fullerene organic solar cells. *Nat. Commun.* **2020**, *11*, 5617.
(22) Liu, J.; Chen, S.; Qian, D.; Gautam, B.; Yang, G.; Zhao, J.; Bergqvist, J.; Zhang, F.; Ma, W.; Ade, H.; Inganäs, O.; Gundogdu, K.; Gao, F.; Yan, H.; et al. Fast charge separation in a non-fullerene organic solar cell with a small driving force. *Nat. Energy* **2016**, *1*, 16089.
(23) Tautz, R.; Da Como, E.; Wiebeler, C.; Soavi, G.; Dumsch, I.; Frohlich, N.; Grancini, G.; Allard, S.; Scherf, U.; Cerullo, G.; et al. Charge photogeneration in donor-acceptor conjugated materials: Influence of excess excitation energy and chain length. *J. Am. Chem. Soc.* **2013**, *135*, 4282.
(24) Wu, J.; Lee, J.; Chin, Y.-C.; Yao, H.; Cha, H.; Luke, J.; Hou, J.; Kim, J.-S.; Durrant, J. R. Exceptionally low charge trapping enables highly efficient organic bulk heterojunction solar cells. *Energy Environ. Sci.* **2020**, *13*, 2422.
(25) Zhong, Y.; Causa', M.; Moore, G. J.; Krauspe, P.; Xiao, B.; Günther, F.; Kublitski, J.; Shivhare, R.; Benduhn, J.; BarOr, E.; Mukherjee, S.; Yallum, K. M.; Réhault, J.; Mannsfeld, S. C. B.; Neher, D.; Richter, L. J.; DeLongchamp, D. M.; Ortmann, F.; Vandewal, K.; Zhou, E.; Banerji, N.; et al. Sub-picosecond charge-transfer at near-zero driving force in polymer:Non-fullerene acceptor blends and bilayers. *Nat. Commun.* **2020**, *11*, 833.
(26) Vandewal, K.; Albrecht, S.; Hoke, E. T.; Graham, K. R.; Widmer, J.; Douglas, J. D.; Schubert, M.; Mateker, W. R.; Bloking, J. T.; Burkhard, G. F.; et al. Efficient charge generation by relaxed charge-transfer states at organic interfaces. *Nat. Mater.* **2014**, *13*, 63.
(27) Ulbricht, R.; Hendry, E.; Shan, J.; Heinz, T. F.; Bonn, M. Carrier dynamics in semiconductors studied with time-resolved terahertz spectroscopy. *Rev. Mod. Phys.* **2011**, *83*, 543.
(28) Bergren, M. R.; Palomaki, P. K.; Neale, N. R.; Furtak, T. E.; Beard, M. C. Size-dependent exciton formation dynamics in colloidal silicon quantum dots. *ACS Nano* **2016**, *10*, 2316.
(29) Steinleitner, P.; Merkl, P.; Nagler, P.; Mornhinweg, J.; Schuller, C.; Korn, T.; Chernikov, A.; Huber, R. Direct observation of ultrafast exciton formation in a monolayer of wse(2). *Nano Lett.* **2017**, *17*, 1455.
(30) Hendry, E.; Schins, J. M.; Candeias, L. P.; Siebbeles, L. D.; Bonn, M. Efficiency of exciton and charge carrier photogeneration in a semiconducting polymer. *Phys. Rev. Lett.* **2004**, *92*, No. 196601.
(31) Parkinson, P.; Lloyd-Hughes, J.; Johnston, M. B.; Herz, L. M. Efficient generation of charges via below-gap photoexcitation of polymer-fullerene blend films investigated by terahertz spectroscopy. *Phys. Rev. B* **2008**, *78*, No. 115321.
(32) Zhang, H.; Wang, X.; Sun, Y.; Han, P.; Ren, J.; Sun, W.; Feng, S.; Ye, J.; Yang, S.; Bester, G.; et al. Effect of it-m doping on charge transfer and ultrafast carrier dynamics of ternary organic solar cell materials. *J. Phys. D-Appl. Phys.* **2020**, *53*, No. 095103.
(33) Melianas, A.; Kemerink, M. Photogenerated charge transport in organic electronic materials: Experiments confirmed by simulations. *Adv. Mater.* **2019**, *31*, No. 1806004.
(34) Pattengale, B.; Neu, J.; Ostresh, S.; Hu, G.; Spies, J. A.; Okabe, R.; Brudvig, G. W.; Schmuttenmaer, C. A. Metal-organic framework photoconductivity via time-resolved terahertz spectroscopy. *J. Am. Chem. Soc.* **2019**, *141*, 9793.
(35) Nyakuchena, J.; Ostresh, S.; Streater, D.; Pattengale, B.; Neu, J.; Fiankor, C.; Hu, W.; Kinigstein, E. D.; Zhang, J.; Zhang, X.; et al. Direct evidence of photoinduced charge transport mechanism in 2d conductive metal organic frameworks. *J. Am. Chem. Soc.* **2020**, *142*, 21050.
(36) Fu, S.; du Fossé, I.; Jia, X.; Xu, J.; Yu, X.; Zhang, H.; Zheng, W.; Krasel, S.; Chen, Z.; Wang, Z. M.; Tielrooij, K. J.; Bonn, M.; Houtepen, A. J.; Wang, H. I.; et al. Long-lived charge separation following pump-wavelength-dependent ultrafast charge transfer in graphene/ws2 heterostructures. *Sci. Adv.* **2021**, *7*, No. eabd9061.
(37) Zhang, H.; Debroye, E.; Zheng, W.; Fu, S.; Virgilio, L. D.; Kumar, P.; Bonn, M.; Wang, H. I. Highly mobile hot holes in cs2agbibr6 double perovskite. *Sci. Adv.* **2021**, *7*, No. eabj9066.
(38) Ohta, K.; Hiramatsu, Y.; Takahashi, K.; Suzuki, M.; Yamada, H.; Tominaga, K. Dynamic behavior of photogenerated charge carriers in diketopyrrolopyrrole-binked tetrabenzoporphyrin-based bulk heterojunction thin films probed with time-resolved terahertz spectroscopy. *J. Photochem. Photobiol. A-Chem.* **2020**, *400*, No. 112693.
(39) Ohta, K.; Tominaga, K.; Ikoma, T.; Kobori, Y.; Yamada, H. Microscopic structures, dynamics, and spin configuration of the charge carriers in organic photovoltaic solar cells studied by advanced time-resolved spectroscopic methods. *Langmuir* **2022**, *38*, 7365.
(40) Ponseca, C. S., Jr.; Yartsev, A.; Wang, E.; Andersson, M. R.; Vithanage, D.; Sundstrom, V. Ultrafast terahertz photoconductivity of bulk heterojunction materials reveals high carrier mobility up to nanosecond time scale. *J. Am. Chem. Soc.* **2012**, *134*, 11836.
(41) Ohta, K.; Tokonami, S.; Takahashi, K.; Tamura, Y.; Yamada, H.; Tominaga, K. Probing charge carrier dynamics in porphyrin-based organic semiconductor thin films by time-resolved thz spectroscopy. *J. Phys. Chem. B* **2017**, *121*, 10157.
(42) Ponseca, C. S., Jr.; Nemec, H.; Vukmirovic, N.; Fusco, S.; Wang, E.; Andersson, M. R.; Chabera, P.; Yartsev, A.; Sundstrom, V. Electron and hole contributions to the terahertz photoconductivity of a conjugated polymer:Fullerene blend identified. *J. Phys. Chem. Lett.* **2012**, *3*, 2442.
(43) Bian, Q.; Ma, F.; Chen, S.; Wei, Q.; Su, X.; Buyanova, I. A.; Chen, W. M.; Ponseca, C. S.; Linares, M.; Karki, K. J.; Yartsev, A.; Inganäs, O.; et al. Vibronic coherence contributes to photocurrent generation in organic semiconductor heterojunction diodes. *Nat. Commun.* **2020**, *11*, 617.
(44) Jin, Z.; Gehrig, D.; Dyer-Smith, C.; Heilweil, E. J.; Laquai, F.; Bonn, M.; Turchinovich, D. Ultrafast terahertz photoconductivity of photovoltaic polymer-fullerene blends: A comparative study correlated with photovoltaic device performance. *J. Phys. Chem. Lett.* **2014**, *5*, 3662.
(45) Wang, K.; Chen, H.; Zhang, J.; Zou, Y.; Yang, Y. Intrachain and interchain exciton-exciton annihilation in donor-acceptor copolymers. *J. Phys. Chem. Lett.* **2021**, *12*, 3928.
(46) Rao, A.; Chow, P. C.; Gelinas, S.; Schlenker, C. W.; Li, C. Z.; Yip, H. L.; Jen, A. K.; Ginger, D. S.; Friend, R. H. The role of spin in the kinetic control of recombination in organic photovoltaics. *Nature* **2013**, *500*, 435.
(47) Wang, R.; Xu, J.; Fu, L.; Zhang, C.; Li, Q.; Yao, J.; Li, X.; Sun, C.; Zhang, Z. G.; Wang, X.; et al. Nonradiative triplet loss suppressed in organic photovoltaic blends with fluoridated nonfullerene acceptors. *J. Am. Chem. Soc.* **2021**, *143*, 4359.
(48) Gillett, A. J.; Privitera, A.; Dilmurat, R.; Karki, A.; Qian, D.; Pershin, A.; Londi, G.; Myers, W. K.; Lee, J.; Yuan, J.; et al. The role of charge recombination to triplet excitons in organic solar cells. *Nature* **2021**, *597*, 666.
(49) Wan, J.; Zeng, L.; Liao, X.; Chen, Z.; Liu, S.; Zhu, P.; Zhu, H.; Chen, Y. All-green solvent-processed planar heterojunction organic solar cells with outstanding power conversion efficiency of 16%. *Adv. Funct. Mater.* **2021**, *32*, No. 2107567.
(50) Giannini, S.; Di Virgilio, L.; Bardini, M.; Hausch, J.; Geuchies, J. J.; Zheng, W.; Volpi, M.; Elsner, J.; Broch, K.; Geerts, Y. H.; et al. Transiently delocalized states enhance hole mobility in organic molecular semiconductors. *Nat. Mater.* **2023**, *22*, 1361.
(51) Lane, P. A.; Cunningham, P. D.; Melinger, J. S.; Kushto, G. P.; Esenturk, O.; Heilweil, E. J. Photoexcitation dynamics in films of c <

sub > 60</sub> and zn phthalocyanine with a layered nanostructure. *Phys. Rev. Lett.* **2012**, *108*, No. 077402.
(52) Chang, G.; Divin, C. J.; Liu, C.-H.; Williamson, S. L.; Galvanauskas, A.; Norris, T. B. Power scalable compact thz system based on an ultrafast yb-doped fiber amplifier. *Opt. Express* **2006**, *14*, 7909.
(53) Kumar, A.; Solanki, A.; Manjappa, M.; Ramesh, S.; Srivastava, Y. K.; Agarwal, P.; Sum, T. C.; Singh, R. Excitons in 2d perovskites for ultrafast terahertz photonic devices. *Sci. Adv.* **2020**, *6*, No. eaax8821.
(54) Cooke, D. G.; Krebs, F. C.; Jepsen, P. U. Direct observation of sub-100 fs mobile charge generation in a polymer-fullerene film. *Phys. Rev. Lett.* **2012**, *108*, No. 056603.
(55) Arkhipov, V. I.; Emelianova, E. V.; Bassler, H. Hot exciton dissociation in a conjugated polymer. *Phys. Rev. Lett.* **1999**, *82*, 1321.
(56) Grancini, G.; Maiuri, M.; Fazzi, D.; Petrozza, A.; Egelhaaf, H. J.; Brida, D.; Cerullo, G.; Lanzani, G. Hot exciton dissociation in polymer solar cells. *Nat. Mater.* **2013**, *12*, 29.
(57) Cai, Y.; Li, Q.; Lu, G.; Ryu, H. S.; Li, Y.; Jin, H.; Chen, Z.; Tang, Z.; Lu, G.; Hao, X.; Woo, H. Y.; Zhang, C.; Sun, Y.; et al. Vertically optimized phase separation with improved exciton diffusion enables efficient organic solar cells with thick active layers. *Nat. Commun.* **2022**, *13*, 2369.
(58) Firdaus, Y.; Le Corre, V. M.; Karuthedath, S.; Liu, W.; Markina, A.; Huang, W.; Chattopadhyay, S.; Nahid, M. M.; Nugraha, M. I.; Lin, Y.; Seitkhan, A.; Basu, A.; Zhang, W.; McCulloch, I.; Ade, H.; Labram, J.; Laquai, F.; Andrienko, D.; Koster, L. J. A.; Anthopoulos, T. D.; et al. Long-range exciton diffusion in molecular non-fullerene acceptors. *Nat. Commun.* **2020**, *11*, 5220.
(59) Chandrabose, S.; Chen, K.; Barker, A. J.; Sutton, J. J.; Prasad, S. K. K.; Zhu, J.; Zhou, J.; Gordon, K. C.; Xie, Z.; Zhan, X.; et al. High exciton diffusion coefficients in fused ring electron acceptor films. *J. Am. Chem. Soc.* **2019**, *141*, 6922.
(60) Cai, Y.; Li, Y.; Wang, R.; Wu, H.; Chen, Z.; Zhang, J.; Ma, Z.; Hao, X.; Zhao, Y.; Zhang, C.; Huang, F.; Sun, Y.; et al. A well-mixed phase formed by two compatible non-fullerene acceptors enables ternary organic solar cells with efficiency over 18.6%. *Adv. Mater.* **2021**, *33*, No. 2101733.
(61) Wang, Y.; Price, M. B.; Bobba, R. S.; Lu, H.; Xue, J.; Wang, Y.; Li, M.; Ilina, A.; Hume, P. A.; Jia, B.; Li, T.; Zhang, Y.; Davis, N. J. L. K.; Tang, Z.; Ma, W.; Qiao, Q.; Hodgkiss, J. M.; Zhan, X.; et al. Quasi-homojunction organic nonfullerene photovoltaics featuring fundamentals distinct from bulk heterojunctions. *Adv. Mater.* **2022**, *34*, No. 2206717.
(62) Jiang, K.; Zhang, J.; Zhong, C.; Lin, F. R.; Qi, F.; Li, Q.; Peng, Z.; Kaminsky, W.; Jang, S.-H.; Yu, J.; et al. Suppressed recombination loss in organic photovoltaics adopting a planar−mixed heterojunction architecture. *Nat. Energy* **2022**, *7*, 1076.
(63) Li, W.; Zeiske, S.; Sandberg, O. J.; Riley, D. B.; Meredith, P.; Armin, A. Organic solar cells with near-unity charge generation yield. *Energy Environ. Sci.* **2021**, *14*, 6484.
(64) Hood, S. N.; Kassal, I. Entropy and disorder enable charge separation in organic solar cells. *J. Phys. Chem. Lett.* **2016**, *7*, 4495.
(65) Monahan, N. R.; Williams, K. W.; Kumar, B.; Nuckolls, C.; Zhu, X. Y. Direct observation of entropy-driven electron-hole pair separation at an organic semiconductor interface. *Phys. Rev. Lett.* **2015**, *114*, No. 247003.
(66) Saladina, M.; Simón Marqués, P.; Markina, A.; Karuthedath, S.; Wöpke, C.; Göhler, C.; Chen, Y.; Allain, M.; Blanchard, P.; Cabanetos, C.; Andrienko, D.; Laquai, F.; Gorenflot, J.; Deibel, C.; et al. Charge photogeneration in non-fullerene organic solar cells: Influence of excess energy and electrostatic interactions. *Adv. Funct. Mater.* **2021**, *31*, No. 2007479.
(67) Li, X.; Zhang, Q.; Yu, J.; Xu, Y.; Zhang, R.; Wang, C.; Zhang, H.; Fabiano, S.; Liu, X.; Hou, J.; Gao, F.; Fahlman, M.; et al. Mapping the energy level alignment at donor/acceptor interfaces in non-fullerene organic solar cells. *Nat. Commun.* **2022**, *13*, 2046.
(68) Schwarze, M.; Schellhammer, K. S.; Ortstein, K.; Benduhn, J.; Gaul, C.; Hinderhofer, A.; Perdigón Toro, L.; Scholz, R.; Kublitski, J.; Roland, S.; Lau, M.; Poelking, C.; Andrienko, D.; Cuniberti, G.; Schreiber, F.; Neher, D.; Vandewal, K.; Ortmann, F.; Leo, K.; et al. Impact of molecular quadrupole moments on the energy levels at organic heterojunctions. *Nat. Commun.* **2019**, *10*, 2466.
(69) Melianas, A.; Pranculis, V.; Xia, Y.; Felekidis, N.; Inganäs, O.; Gulbinas, V.; Kemerink, M. Photogenerated carrier mobility significantly exceeds injected carrier mobility in organic solar cells. *Adv. Energy Mater.* **2017**, *7*, No. 1602143.
(70) Liu, Y.; Zhao, J.; Li, Z.; Mu, C.; Ma, W.; Hu, H.; Jiang, K.; Lin, H.; Ade, H.; Yan, H. Aggregation and morphology control enables multiple cases of high-efficiency polymer solar cells. *Nat. Commun.* **2014**, *5*, 5294.
(71) Foster, S.; Deledalle, F.; Mitani, A.; Kimura, T.; Kim, K.; Okachi, T.; Kirchartz, T.; Oguma, J.; Miyake, K.; Durrant, J. R.; Doi, S.; Nelson, J.; et al. Electron collection as a limit to polymer:Pcbm solar cell efficiency: Effect of blend microstructure on carrier mobility and device performance in ptb7:Pcbm. *Adv. Energy Mater.* **2014**, *4*, No. 1400311.
(72) Bakulin, A. A.; Rao, A.; Pavelyev, V. G.; van Loosdrecht, P. H. M.; Pshenichnikov, M. S.; Niedzialek, D.; Cornil, J.; Beljonne, D.; Friend, R. H. The role of driving energy and delocalized states for charge separation in organic semiconductors. *Science* **2012**, *335*, 1340.
(73) Gelinas, S.; Rao, A.; Kumar, A.; Smith, S. L.; Chin, A. W.; Clark, J.; van der Poll, T. S.; Bazan, G. C.; Friend, R. H. Ultrafast long-range charge separation in organic semiconductor photovoltaic diodes. *Science* **2014**, *343*, 512.

https://doi.org/10.1021/jacs.4c05786
J. Am. Chem. Soc. 2024, 146, 20312−20322